Experimental and numerical investigation of extrudate swell of polylactic acid via Extrusion-based Additive Manufacturing process

Hong Wang, Faleh Rabhi, Abel Cherouat, Alexandre Gilbin, Thierry Barriere

Experimental and numerical investigation of extrudate swell of polylactic acid via Extrusion-based Additive Manufacturing process

H. Wang[1, 2], F. Rabhi[2], A. Cherouat[1], A. Gilbin[3], T. Barriere[2]

[1]Univ. of Technology of Troyes, GAMMA3, 12 Rue Marie Curie, Troyes, 10004, France

[2] Université de Franche-Comté, SUPMICROTECH, CNRS, institut FEMTO-ST, F-25000 Besançon, France

[3] SUPMICROTECH, CNRS, institut FEMTO-ST, F-25000 Besançon, France

Abstract

Extrusion swell is a rheological phenomenon of polymers that occurs after the extrusion die exit due to relaxation of the residual molecular stress. This phenomenon is essential to ensure the accuracy and stability of components manufactured by Extrusion-Based Additive Manufacturing (EAM) process. Extrudate swell can be affected by multiple factors including material properties and processing parameters that can be coupled and it is difficult to fully understand their effects, especially in absence of accurate online measurement devices. In this study, we investigated experimentally the extrudate swell as a function of the extrusion rate, melt temperature and nozzle diameter for polylactic acid (PLA) material. The Computational Fluid Dynamics (CFD) and Level Set (LS) method in COMSOL Multiphysics were used to simulate the polymer flow out of the extrusion nozzle. The simulation results matched well with experimental results and showed that the swell rate decreases with increasing temperature and nozzle diameter and decreasing extrusion rate. These results can be used to optimize the parameters of EAM processes.

Keywords: EAM; Extrudate swell; Polylactic Acid; Level Set method; Experiment.

Notations

a	Transition factor	
c_p	Heat capacity	J K^{-1} kg^{-1}
D_e	Diameter of the extrudate	m
D	Die diameter	m
E_a	Activation energy	J mol^{-1}
g	Acceleration of gravity	m s^{-2}
k	Thermal conductivity	W m^{-1} K^{-1}
L	Length of the extrudate	m
n	Pseudo plasticity index	
p	Pressure	MPa
V	Imposed inlet velocity	MPa
R	Molar constant of perfect gases	J mol^{-1} K^{-1}
B	Swelling ratio	
t	Time	s
T	Temperature	K
T_m	Imposed temperature	K
T_f	Melting temperature	K
T_g	Glass transition temperature	K
u	Velocity field	m s^{-1}
α_{air}	Thermal air diffusion	m^2 s^{-1}
$\alpha_{polymer}$	Thermal diffusion of polymer	m^2 s^{-1}
ε_{ls}	Interface thickness control parameter	m
γ	Reset parameter	m s^{-1}
$\dot{\gamma}$	Shear rate	s^{-1}
ϕ	Volume fraction	
λ	Characteristic time	s
ρ	Density	kg m^{-3}
η_∞	Infinite shear viscosity	Pa s
η_0	Zero shear viscosity	Pa s
η	Viscosity	Pa s

1 Introduction

Extrusion-based Additive Manufacturing (EAM) [1], one of the most widely used Additive Manufacturing (AM) processes, involves extruding materials in their molten state through a die/nozzle and depositing them layer by layer to build complex shapes. The materials can be thermoplastics polymers [2][3] or feedstocks composed of a binder and metal [4][5] or ceramic powders [6], in filament or pellet shape. Compared to other AM processes, EAM processes use low-cost equipment and allows a wide range of materials to be selected.

Extrudate swell is considered as a flow instability phenomenon describing the rise of extrudate diameter compared to the die diameter and it can be also called die swell or Barus effect. When the polymer melts flow through a contraction regime, they undergo shear and extensional forces and the chains are more stretched and later gain recoiling immediately after existing the flow channel, which results in a decrease of flow velocity along the flow direction and this velocity reconstruction leads to the increase of the extrudate diameter. Thus, the extrusion swell relates to the viscoelasticity of the material. The degree of the extrusion swell is usually quantified by the ratio of the extrudate diameter versus die diameter.

Extrudate swell can be affected by multiple factors, such as temperature, die geometry, extrusion stress and molecular weight of the polymer [7]. For example, Liang et al. [8] used a capillary rheometer to measure the die swell ratio of polypropylene (PP). Upon increasing the shear rate, the swell ratio increased sharply at low shear rate and then gradually reached the maximal value at the highest shear rate. When the shear rate was fixed, the swell ratio decreased with a rise of temperature. Anand et al. [9] reported the extrudate swell of PP melts with capillary dies of various length to diameter L/∅D ratios. They found that the swell ratio decreased with increasing the L/∅D ratio when the shear rate is fixed. Behzadfar et al. [10] used a capillary die with different L/∅D ratio and entrance angle to assess the extrusion swell ratio. They found that the swell ratio decreased with a rise of L/∅D ration and decreased with increasing the entrance angle until to 180°. Thus, it's essential to control the die swell especially in applications that require high precision and dimensional stability.

In order to understand the relation of viscoelasticity, processing conditions and swelling, the experimental data of die swell is essential. Early research attempt to measure the extrudate swell with pinch-off method [11] [12] [13] that the extrudate is frozen for measurement. However, this method is inaccurate as it involves the error resulted from cooling and solidifying. More accurate methods include the use of in-time equipment like infrared transmission and optical cameras [14] [15].

Numerical modeling is recommended to investigate the extrudate swell as it gives insights into the flow behavior inside and outside the flow channel. In the 1970s, Tanner [16] developed a Tanner analytical method that allows the estimation of the extrudate swell ratio assuming that the die has infinite length. Tang et al. [17] used finite element method including a differential multimode Phan-Thien-Tanner (PTT) constitutive model to simulate extrudate swell of polypropylene through slit dies. They found that increasing the width/height ratio from 1 to 20 contributed to 10-30% extrudate deformation in different directions and delayed the equilibrium position along the flow direction. Konaganti et al. [18] used viscoelastic constitutive models, a 6-mode integral Kaye-Bernstein–Kearsley–Zapas (K-BKZ) model and a differential PTT model, to investigate the extrudate swell of a molten high-density polyethylene (HDPE) through capillary dies. They found that extrudate swell decreases with increasing temperature, apparent shear rate and the L/∅D ratio. However, the K-BKZ model overestimated and

the PTT model underpredicted the experimental results, leading to an unexplained problem. Most research focused on the capillary dies with long L/∅D ratio compared to nozzles used in EAM processes.

In this study, an online method using a high-definition camera and a thermal camera to capture the extrusion swell and temperature distribution downstream of the nozzle exit was adopted. Processing parameters such as temperature, extrusion rate and nozzle diameter of an EAM printer were studied. The experimental results were fed into the Two-Phase Flow module of the COMSOL Multiphysics software with the Level-Set (LS) method to model the extrusion swell phenomenon. These results and analyses were used to predict and optimize the extrudate swell in EAM process.

2 Experimental materials and methods

2.1 Material used

Polylactic acid (PLA) is the most widely used polymer in the EAM applications [19] due to its biodegradability and environmental properties. The PLA (PLI005, Natureplast, France) was used in this study to characterize extrudate swell during EAM process. Differential Scanning Calorimetry (DSC) was used to analyze the thermal properties of PLA. Their physical and thermal properties are shown in Table 1.

Table 1 Physical and thermal properties of PLA.

Polymer	PLA
Density $\boldsymbol{\rho}$ (g.cm^{-3})	1.25
Heat capacity $\boldsymbol{c_p}$ (J.kg^{-1}.K^{-1})	2100
Thermal conductivity $\boldsymbol{k}$ (W.m^{-1}.K^{-1})	0.205
Glass transition temperature $\boldsymbol{T_g}$ (℃)	52 - 65
Melting temperature $\boldsymbol{T_f}$ (℃)	169 - 179

2.2 Measurements of rheological behaviors and modeling

The shear viscosity of PLA in the molten state was characterized to determine the rheological behaviour using a plane-cone rotational rheometer (HAAKE MARS 60 Rheometer) for low shear rates and a capillary rheometer (Rosand RH2000) for high shear rates.

The experimentally measured viscosity as a function of shear rate for temperature range of 180-220℃ is shown in Fig.1. The shear viscosity decreases with increasing the temperature and shear rate, illustrating that the PLA has a thermally dependent pseudoplastic type of rheological behaviour in our case.

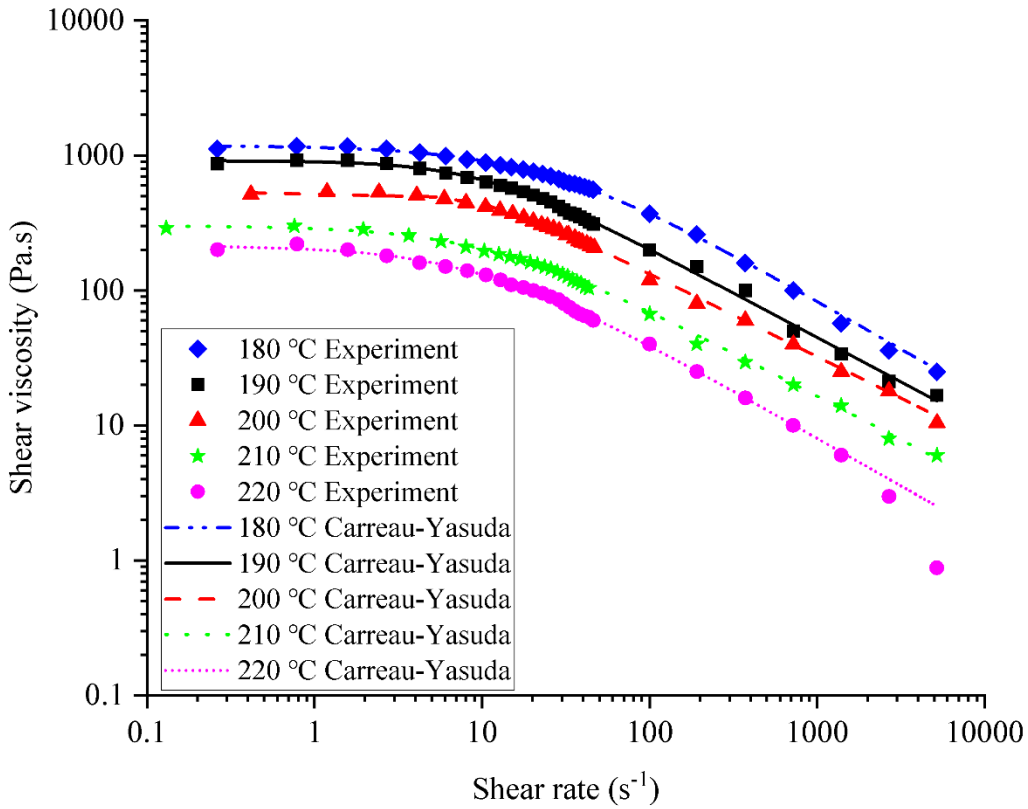

Fig.1 Shear viscosity vs. shear rate curve of PLA.

The Carreau-Yasuda model which accounts for both the Newtonian regime (constant viscosity at low shear rate) and shear-thinning regime (viscosity decreases with increasing the shear rate) was used as the rheological model and Arrhenius model was used to account for temperature. The shear viscosity $\eta(\dot{\gamma},T)$ and the two models are expressed in equations:

$$\eta(\dot{\gamma},T) = a_T \eta(\dot{\gamma},T_0) \tag{1}$$

$$\eta = \eta_\infty + (\eta_0 - \eta_\infty)(1+(\lambda\dot{\gamma})^a)^{\frac{n-1}{a}} \tag{2}$$

$$a_T = \exp\left[\frac{E_a}{R}\left(\frac{1}{T}-\frac{1}{T_0}\right)\right] \tag{3}$$

where η_0 is the viscosity for zero shear rate, η_∞ the viscosity at infinite shear rate, λ the characteristic time of the material, a the parameter adjusting the transition regime between the Newtonian plateau and the shear-thinning regime, n the pseudo-plasticity index, $\dot{\gamma}$ the shear rate, T the temperature, T_0 the reference temperature (here was 190 $°C$), E_a the activation energy and R the gas constant.

The values of the identified parameters were obtained by the least square method using the experimental data and are summarized in Table 2. The value of the pseudoplastic index n (<1) indicates that the PLA is pseudoplastic.

Table 2 Summary of the identified parameters of Carreau-Yasuda law and Arrhenius law.

T (℃)	η_0 (Pa s)	η_∞ (Pa s)	λ (s)	n	a	E_a (kJ mol^{-1})
180	1187	0	0.04	0.28	0.96	105.83
190	917	0	0.10	0.34	1.35	

200	535	0	0.08	0.33	1.66
210	302	0	0.09	0.35	1.05
220	216	0	0.10	0.29	1.01

2.3 Experimental characterization of die swell and temperature distribution

A dynamic camera (Basler Ace acA3088) with a macro lens was used to measure the extrudate swell and an infrared camera (Optris PI 450i) was selected to quantify the temperature of the extrudate. Both cameras were installed perpendicular to the extrudate flow direction as shown in Fig.2.

The EAM (printing) equipment is a screw-based 3D printer in which the material is fed and extruded by the rotation of a single screw from thermoplastic polymer pellets. For each photograph, the outline of the extrudate was detected using ImageJ after calibration by an object of known size placed in the same plane where the extrudate flowed perpendicular to the camera.

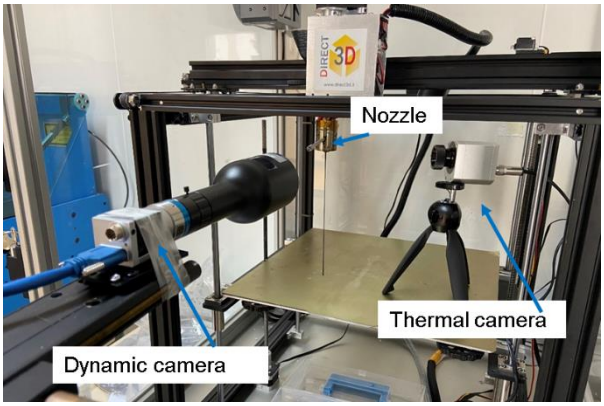

Fig.2 The setup of the dynamic and the infrared cameras.

Before the measurements of the temperature, the emissivity of PLA was determined by adjusting the emissivity of the thermal camera to achieve the same temperature captured by the thermal couple which was placed on the surface of the melted materials. A small control region of 3×3 pixels was selected near the die exit to measure the extrudate temperature and three other areas were selected to evaluate the evolution of temperature along with the extrudate, as shown in Fig.3(a). When PLA flows out of the nozzle exit, it undergoes a creep phenomenon that it deforms (expansion) to relax the build-up residual stresses generated by the shear and compression forces to the polymer chain network during extrusion through the extruder. With contact to the nozzle surface, the expanded material forms a bulb at the onset of the extrusion. As the extrudate flows, the bulb leaves the nozzle surface and the hanging mass of the extrudate results in an apparent necking. Both the bulb and necking part are not suitable for charactering the extrudate swell. The extrudate swell **was** measured at the top of the extrudate where the extrudate **swelled** to the maximal diameter.

As the extrudate **flowed** downward past the observation points (P1-P4), the temperature at each point as a function of time **was** recorded in real-time, as shown in Fig.3(b). The curves can be divided into three domains. In the extrudate arrival domain, the temperature remains the ambient temperature until the arrival of the extrudate, except for P1, which starts at a higher temperature because it is right under the nozzle and has already some residual PLA. The unsteady state represents the variation of temperature resulting from the extrusion process that the newly fed cooler material exchanges the heat or mix with the material that in front of it. As the material of higher temperature

heated in the static state is extruded out, the temperature evolution becomes stable and then the measurement of extrudate swell is started in this steady state. The measurement of extrudate swell started after the stabilization of the temperature profile. In order to maintain the consistency of the die swell, before each measurement when the extrudate **reached** its thermal steady state, the extrudate under the nozzle **was** clipped without stopping the extrusion process. The maximal diameter of the extrudate within 2mm below the nozzle exit when the extrudate **reached** a total length of 6mm **was** measured for determining the die swell.

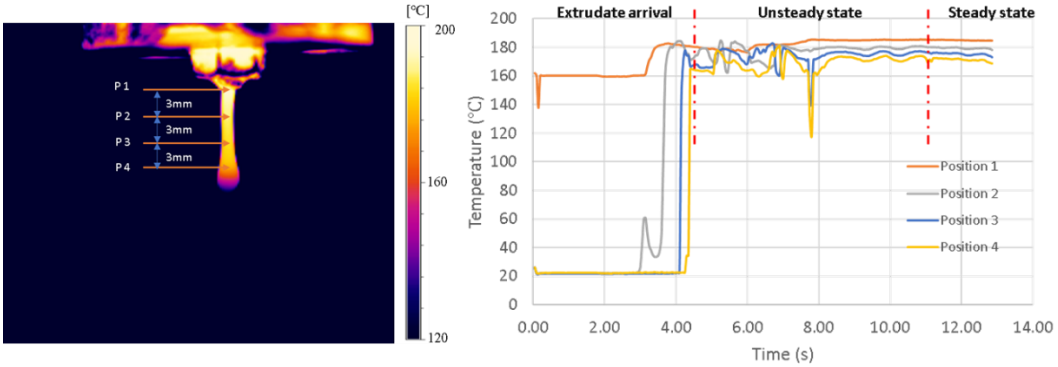

Fig.3 Temperature measurement (a)Position of the measure points along the extrudate (b) Evolution of temperature for PLA at 200 ℃ and V=20 rpm (zoom sur la figure (a) et enlever la partie noir).(figure b P1 P2)

Temperatures of 190℃, 200℃ and 210℃ were tested, and each temperature was related to four extrusion rates (Rotation speed of the screw at 10, 20, 30 and 40 rpm). Two nozzles with different diameters (∅D=0.76mm and ∅D=1.56mm) were studied for comparison. Unlike the filament-used EAM process where the extrusion rate is explicit, the extrusion rate of the pellet-used EAM process using a single screw to extruder the pellets represents only the rotation speed of the screw. So, during each measurement, the mass of the extrudate was recorded for converting to material's volume flow rate.

3 Finite element simulation

3.1 Numerical models

The level-set method LS is a numerical technique for tracking interfaces and shapes using a fixed mesh. The level-set method LS was developed in 1979 by Alain Dervieux [20], and subsequently popularized by Stanley Osher and James Sethian [21] [22]. It has become popular in many disciplines, such as image processing, optimization and computational fluid dynamics.

The interface is represented by an isocontour of a globally defined function, the level set function ϕ. Let a domain $\Omega(t) \in R^3$ with boundary Γ defined by a Level Set function $\phi(x)$. This function is assumed to take positive values inside the region delimited by the curve Γ and negative values outside. In order to investigate the flow in the domain Ω, let the level set function divide the domain in two parts $\Omega = \Omega^+ \bigcup \Omega^-$, where:

$$\begin{cases} \phi(t,x) > 0 & x \in \Omega^{+} \\ \phi(t,x) = 0 & x \in \Gamma \\ \phi(t,x) < 0 & x \notin \Omega^{-} \end{cases} \tag{4}$$

If the curve $\Gamma(t,x)$ moves in the normal direction $n(x) = \dfrac{\nabla\phi}{|\nabla\phi|}$ with a speed $\boldsymbol{u}$, then the level-set function satisfies the level-set equation to solve advection equation to propagate $\phi = 0$ as:

$$\frac{\partial\phi(t,x)}{\partial t} + \boldsymbol{u}(t,x)\nabla\phi = 0 \tag{5}$$

Given at time t = 0, $\phi(0,x) = \phi_0$ for initial domain $\Gamma(0)$ is given, and its motion over time, it is possible to know $\phi(t,x)$ at any time using a second-order in time Runge Kutta scheme as:

$$\begin{cases} \phi_{t+\Delta t} = \phi_t - \Delta t\,(\boldsymbol{u}_t\nabla)\phi_t \\ \phi_t \ \textit{given} \end{cases} \tag{6}$$

The numerical simulations were carried out with the Two Phase Flow (TPF) solver of Level Set (LS) method in COMSOL Multiphysics based on finite element method. D. Kazmer et al. [23] characterized the compressibility of ABS in the material extrusion process with an instrumented hot end design and stated that the compressibility effects can be significant on the transient variances in material extrusion. In this study, the compressibility was not considered and we assumed that the polymer flow is incompressible and the external forces are negligible compared to the internal forces, the Navier-Stocker equations (7) and (8) governing the viscous flow and the LS transport equation (9) tracking the interface between two immiscible fluids are expressed as follows:

$$\rho\left(\frac{\partial\boldsymbol{u}}{\partial t} + \boldsymbol{u}\cdot\nabla\boldsymbol{u}\right) = -\nabla p\boldsymbol{I} + \rho\boldsymbol{g} + \nabla\cdot\left[\eta(\nabla\boldsymbol{u} + \nabla^{T}\boldsymbol{u})\right] \tag{7}$$

$$\nabla\cdot\boldsymbol{u} = 0 \tag{8}$$

$$\frac{\partial\phi}{\partial t} + \nabla\cdot(\boldsymbol{u}\phi) = \gamma\nabla\cdot\left(\varepsilon_{ls}\nabla\phi - \phi(1-\phi)\frac{\nabla\phi}{|\nabla\phi|}\right) \tag{9}$$

where ρ is the fluid density, $\boldsymbol{u}$ the velocity vector, p the pressure, η the dynamic viscosity, $\boldsymbol{g}$ the acceleration of gravity, $\boldsymbol{I}$ the identity vector, ϕ the volume fraction of the fluids varying between 0 and 1 across the free surface and is constant at 0 or 1 in the bulk of the two fluids (the value of 0.5 is assigned to the interface between the polymer and the air), t the time, γ the reset parameter and ε_{ls} the interface thickness control.

In order to model the heat transfer in the flow simulation, the advection-diffusion equation (10) is added by using a partial differential equation (PDE) in COMSOL:

$$\frac{\partial T}{\partial t} + (\boldsymbol{u}\cdot\nabla)T = \left(\frac{k}{\rho c_p}\right)\nabla^{2}T \tag{10}$$

where T is the temperature, k the thermal conductivity, c_p the heat capacity of the fluid. The term $\alpha = \dfrac{k}{\rho c_p}$ represents the thermal diffusivity α within the polymer/air interface and is expressed (same principle for density and viscosity) in (11):

$$\alpha(\phi) = \phi\alpha_{air} + (1-\phi)\alpha_{polymer} \tag{11}$$

where α_{air} and $\alpha_{polymer}$ represent the diffusivity of air and polymer respectively.

The simulation for predicting the extrudate swell at the nozzle exit is realized by coupling different modules in COMSOL Multiphysics software, as illustrated in Fig.4.

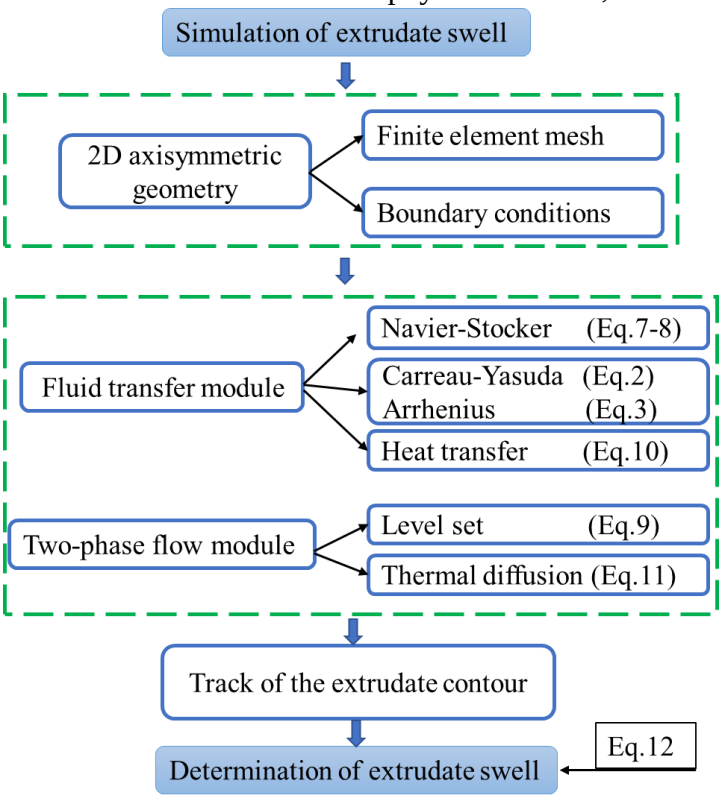

Fig.4 Schema of simulation implementation for extrudate swell.

3.2 Geometrical modeling, boundary conditions and computational grid

The extrusion simulation of PLA was modeled as 2D axisymmetric and the geometry is shown in Fig.5. The yellow part is the nozzle channel filled initially by melted polymer and the green part is the air domain where enters then the polymer. The nozzle radius is R=0.38 mm or 0.78 mm and the nozzle length is L=0.6 mm.

The boundary conditions are shown in Fig.5, including no slip condition and constant extrusion temperature T_m on inner wall of the nozzle, ambient pressure on the outlet and environment temperature T_{env} (25 °C) in the air cavity.

In fact, the volumetric flow rate is not a constant value for a given rotation speed of the screw, but also denpends on the temperature and nozzle geometry. Besides, the realistic extrusion temperature varies with the rotation speed. Thus, the input boundary conditions of inlet velocity V and extrusion temperature T_m were assigned corresponding to each experimental conditions.

The 2D computational grid is physics-controlled meshed (67241 elements) with free triangles and refined in the nozzle contraction region, as shown in Fig.5. Fine mesh size is chosen at the interface polymer-air (55461 elements in the area 2 and 10138 elements in the area 3) and at a very refined mesh (1642 elements) is performed at the exit of the nozzle extruder (area 1).

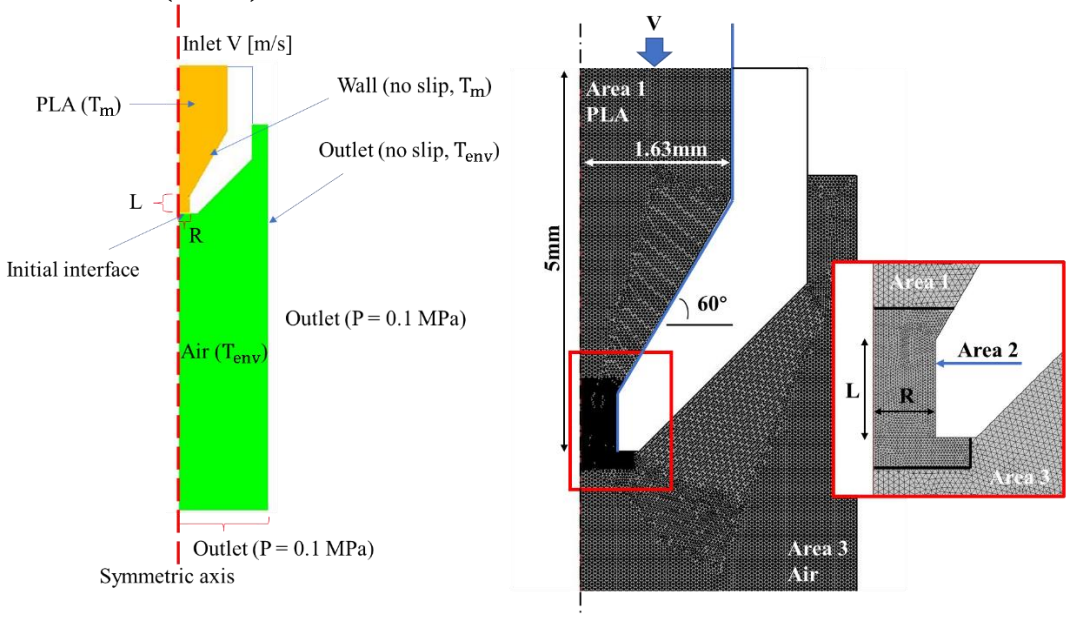

Fig.5 Geometry of simulation model, boundary conditions and computational grid.

4 Results

4.1 Effects of extrusion rate, nozzle diameter and extrusion temperature on the exit temperature and volume flow rate

The printing process parameters used (extrusion temperature, nozzle diameter and extrusion rate) to study the die swelling phenomenon are defined in Table 3.

Fig.6(a) shows the evolution of volume flow rate as a function of the extrusion rate. It also showed the effect of nozzle diameter and extrusion temperature. The slope can be considered as a factor indicating the feeding facility. The feeding process can be considered as a confrontation process of the shear force driven by screw against the force due to the pressure drop inside the nozzle. Nozzle with larger diameter at higher extrusion temperature possesses a high slope. Flowing through a smaller nozzle diameter and under lower temperature, the melt undergoes higher shear force, which hinders the feeding of the material. For instance, the slope of PLA with nozzle diameter ∅=1.56mm at 210 ℃ is 0.85, higher than that (0.28) of nozzle diameter ∅=0.76mm at 190 ℃. Hyvärinen et al. [24] reported that the extrudate flow rate will tend to decrease with screw extrusion rate due to the increased slip at the screw, which was not detected in our study.

Fig.6(b) shows the evolution of exit temperature as a function of the extrusion rate for different nozzles and extrusion temperatures. The exit temperature tends to decrease as the extrusion rate increases, which can be explained by the reduction of the residence time of the material to heat inside the extrude. A larger nozzle diameter facilitates the material flow, which also reduces the residence time inside the extruder. Reasonably, a higher extrusion temperature results in a higher exit temperature.

Table 3 Effects of processing parameters on the extrudate swell phenomenon.

Processing parameter	Parameter values	Volume flow rate (mm^3/s)	Exit temperature (℃)
Extrusion temperature (℃)	T1=190 T2=200 T3=210	**Fig.6**(a) Effect of nozzle diameter, extrusion rate and extrusion temperature on the volume flow rate	**Fig.6**(b) Effect of nozzle diameter, extrusion rate and extrusion temperature on the volume flow rate on the exit temperature
Nozzle diameter (mm)	D1=0.78 D2=1.56		
Extrusion rate (rpm)	R1=10 R2=20 R3=30 R4=40		

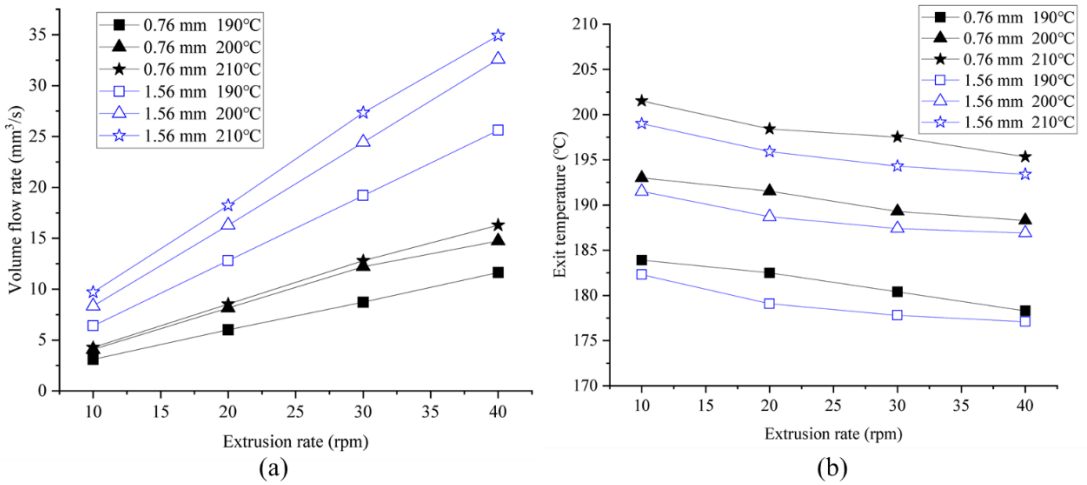

Fig.6 Effects of extrusion temperature, nozzle diameter and extrusion rate on (a) volume flow rate; (b) exit temperature.

In contrast to the assumption of the filament-used EAM processes that the volume flow rate of the melt is proportional to the feeding rate in conditions that the friction force of the extruder gear wheels do not exceed the strength of the filament material and the melt is incompressible, the feeding force in pellet-used EAM is driven by the friction and compression of the material, which results the feeding rate of the pellets a non-linear parameter in relation to the processing parameters. Thus, to reflect the actual feed rate, the extrusion rate is represented by the corresponding volume flow rate. The evolution of exit temperature in **Fig.6**(b) is replotted as a function of volume flow rate in **Fig.7**.The measured nozzle exit temperatures for PLA were lower than the assigned temperature, which is consistent with what has been reported in [25][26]. This is due to the fact that the heat transfer between the liquefier walls and the material is insufficient for the material to reach its assigned temperature. At the same time, as the flow rate increases, the difference between the extrusion temperature and the outlet temperature increases. This is because a higher extrusion rate results in a shorter residence time for the material to pass through the liquefier, making the temperature difference more pronounced. Different nozzles have different volume flow rate under the same processing parameters, but it is interesting to note that their exit temperatures are close in the volume flow rate overlap region, indicating that the reduced exit temperature is primarily due to the volume flow.

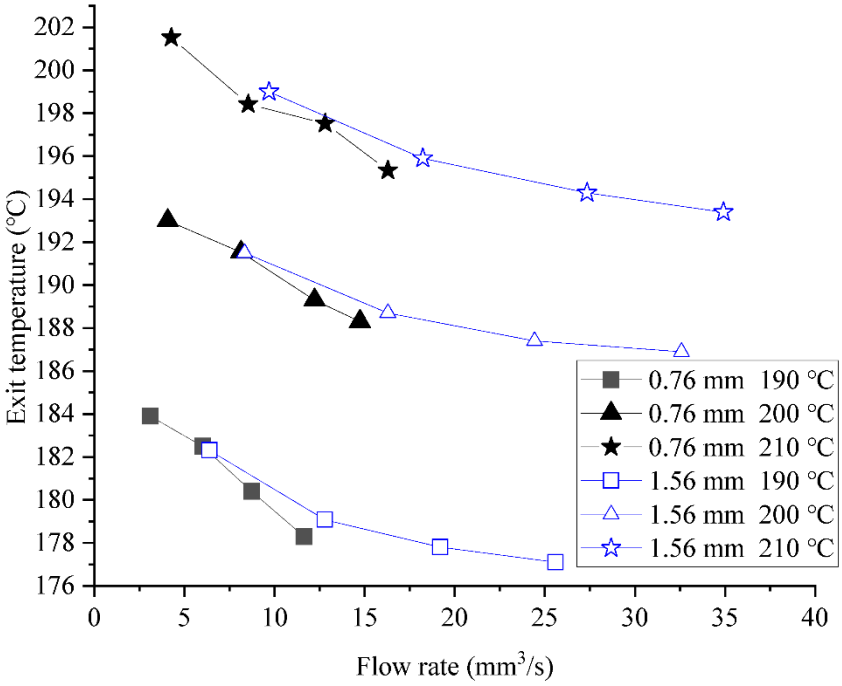

Fig.7 The effect of flow rate and extrusion temperature on the exit temperature

According to the above-mentioned analysis, it turns out to be necessary to account for the real exit temperature and volume flow rate at their stable state for the input of finite element simulation, though the presentation of the results utilize still the assigned values.

4.2 Comparison of the experimental and numerical swell

In our work, the experimental results obtained from the die swelling with two nozzle geometries of different diameter were supported with Tanner's model. He modeled the die swelling (B) as a function of the shear stress τ_p at the wall as described by equation (12), which can also be expressed as a function of the shear rate $\dot{\gamma}$ as equation (13):

$$B = A + (1 + C\tau_p^2)^m \tag{12}$$

$$B = A + (1 + C\dot{\gamma}^2)^m \tag{13}$$

The parameters A, C and m are identified by the least squares method and shown in Table 4. The experimental and Tanner model results of die swell ratio versus shear rate for both nozzles are shown in Fig.8.

The evolution of swelling as a function of shear rates obtained from the experimental point of view correlates well with the results obtained by the Tanner model. For the largest die diameter, the die swell ratios are close to the Newtonian limit of the die swell rate of 1.1, indicating that under the processing conditions, PLA exhibits more non-Newtonian viscous behavior than elastic behavior. For a nozzle diameter of 0.76mm, the die swell ratio is well above 1.1 indicating viscoelastic behavior.

Table 4 Parameters of die swell model of Tanner as a function of shear rate.

Nozzle diameter	A	B	m	R
D1=0.76mm	0.1000	0.0059	0.0205	0.9879
D2=1.56mm	-0.0141	0.0687	0.0201	0.9990

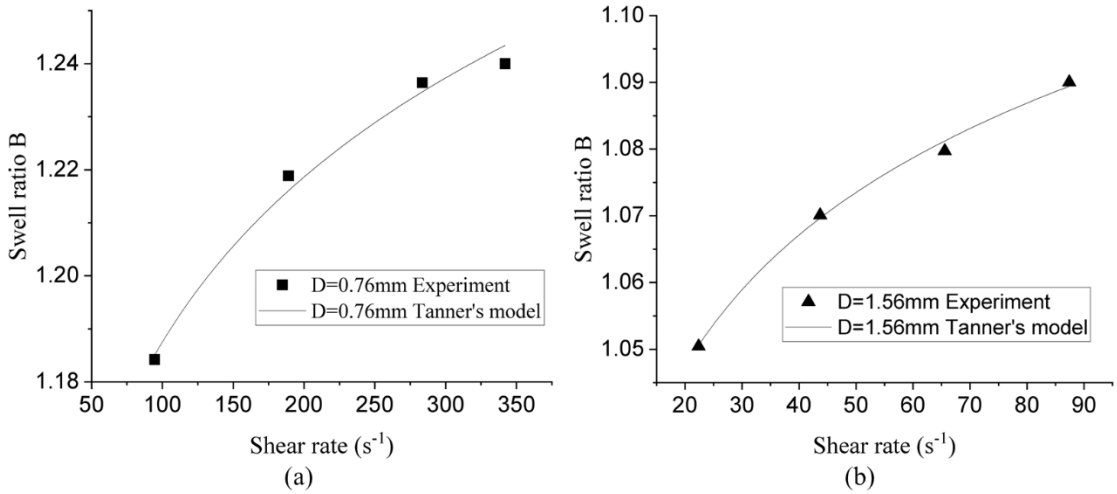

Pas coherent avec figures 11 et 12 poru swell ratio B oiu swell ratio

Fig.8 Experimental results and Tanner's model of die swell ration as a function of shear rate for nozzle diameter of (a) D=0.76mm and (b) D=1.56mm.

A comparison of experimental and numerical results for PLA at extrusion temperature T=200 ℃,extrusion rate of V=20 rpm for nozzle diameter of ∅=0.76 mm is shown in Fig.9. Fig.9(a) shows the temperature distribution captured by the thermal camera as well as the temperature field of simulation (in red dotted box), both revealed the cooling behavior of the extrudate along the flow direction while the simulation results gave an insight to the cooling behavior from the center to the edge. However, the temperature on the surface of the extrudate in simulation seems to reduce faster than the experimental results. The temperature contour in both cases cannot reflect the true contour of the extrudate swell. Fig.9(b) shows the extrudate shape captured by the dynamic camera as well as the field of volume fraction ϕ of PLA (ϕ=1, red) in simulation (in red dotted box). After a sharp swelling, the diameter of the extrudate increases gradually to a stable regime where indicates the arrow. The summary of the results of experiment and simulation is listed in Table 5. The extrudate swell is usually characterized by swell ratio B:

$$B = \frac{\varnothing D_e}{\varnothing D} \tag{14}$$

where $\varnothing D_e$ is the extrudate diameter and $\varnothing D$ the nozzle diameter.

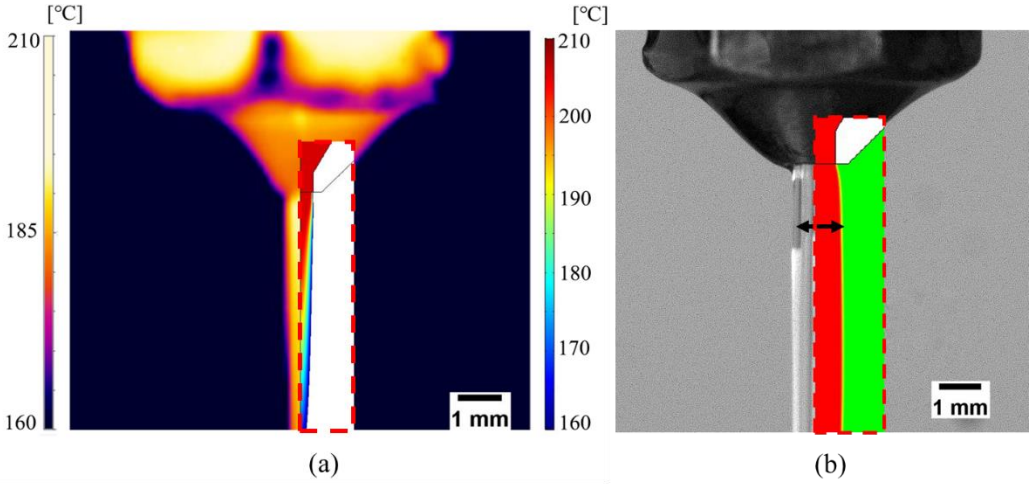

Fig.9 Experimental and numerical results for PLA at 200 ℃, 20 rpm (a) Temperature field captured by thermal camera (simulation result in dotted box); (b) Extrudate contour captured by dynamic camera (simulation result in dotted box).

Table 5 Comparison of extrudate swell ratio between experimental and numerical results for PLA at 200℃.

D=0.76mm	Volume flow rate (mm^3/s)	4.07	8.15	12.22	14.74
	B of experiment	1.18	1.22	1.23	1.24
	B of simulation	1.19	1.24	1.27	1.27
	Error (%)	0.85	1.64	3.25	2.42
D=1.56mm	Volume flow rate (mm^3/s)	8.34	16.29	24.44	32.58
	B of experiment	1.05	1.07	1.08	1.09
	B of simulation	1.06	1.09	1.11	1.12
	Error (%)	0.95	1.81	2.64	2.68

Fig.10 presents the transient behavior of the extrudate at 200 ℃ with nozzle diameter D=0.76mm. The color contour represents here the volume fraction of level set equation, the value of 0.5 is regarded as the interface of PLA and air. The extrudate creeps a bit during the initial flow but didn't form a bulb as obvious as that described in **Fig.3**(a) in lack of a precise initialization. Logically, higher volume flow rate leads to longer lengh and more significant die swell at the same time due to the higher shear rate experienced in the nozzle. As the extrudate continues flowing, it undergoes a fast and significant swelling right out of the nozzle exit and tends to equilibrate between the creep behavior and the tension forces from the hanging mass, after that, the diameter of the extrudate decreases in the flow direction due to the gravity effect.

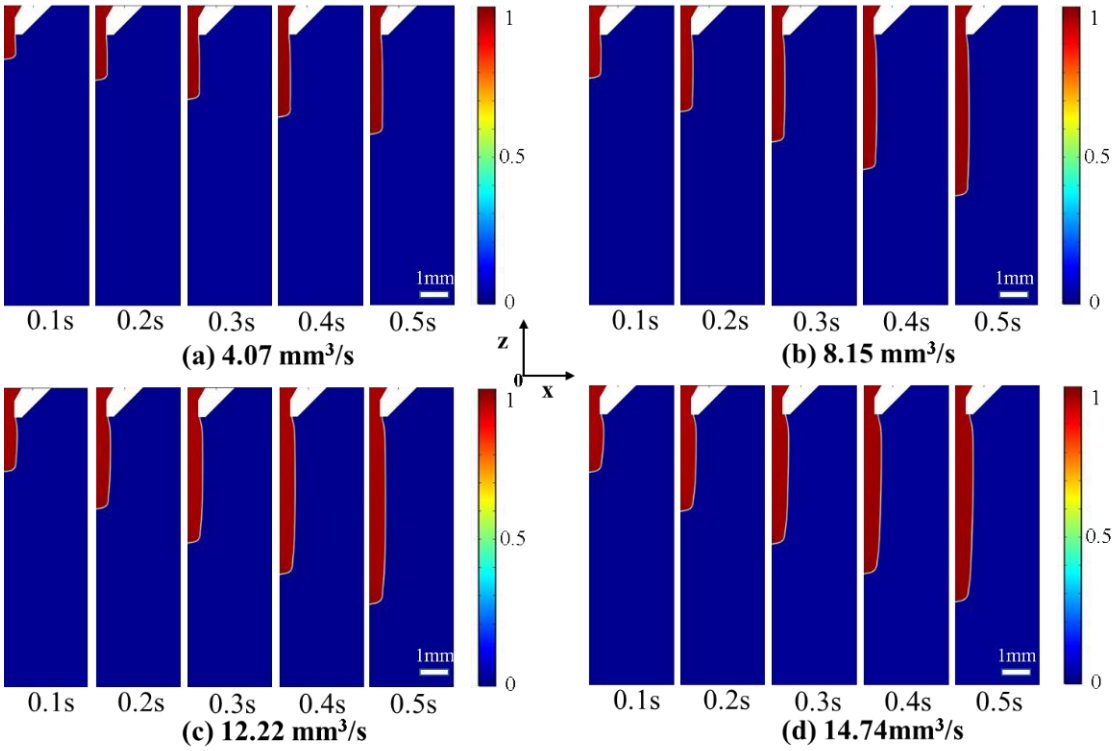

Fig.10 Transient behavior of the extrudate at 200℃ for nozzle diameter of 0.76mm at volume flow rate of (a) 4.07 mm^3/s; (b) 8.15 mm^3/s;(c) 12.22 mm^3/s;(d) 14.74 mm^3/s.

Fig.11 compares the swell ratio between experimental and numerical results as a function of the flow rate at 200℃, which shows that the swell ratio increases with increasing the flow rate for both nozzles. The nozzle of larger diameter has lower swell ratio, which is in accordance with literature [26].

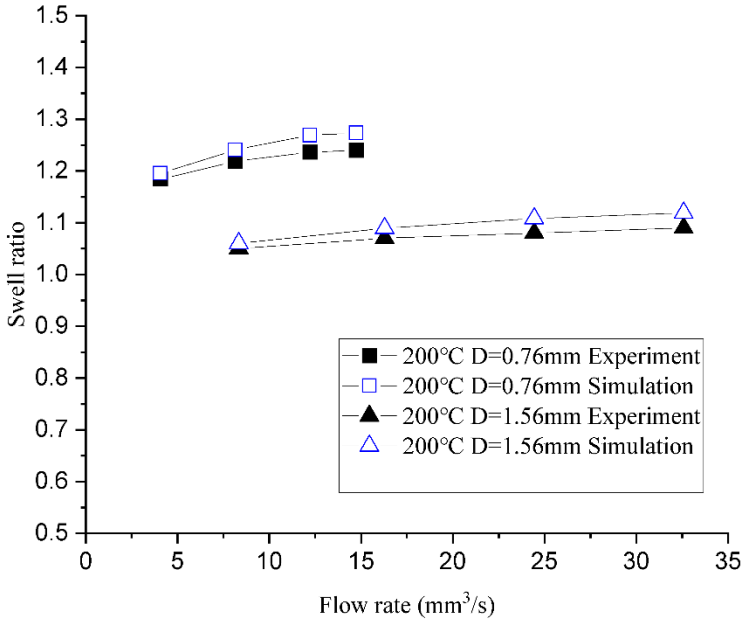

Fig.11 Comparison of experimental and simulation results of die swell for two nozzles at different flow rate and at extrusion temperature of 200℃

Fig.12 shows that the swell ratio decreases with increasing the temperature. This can be explained by the effect of temperature on the polymer chain mobility that the higher temperature promotes the movement of polymer chains and contributes to their reorientation and release of deformation resulted from the shear and compression forces in extrusion. The deviation between the simulation results and experimental results is within 4%, which proves that the simulation correlates well with the experimental results and can be used to investigate and optimize the processing parameters. According to the above results, it can be concluded that reducing the extrusion swell can be achieved by decreasing the extrusion rate, increasing the extrusion temperature and nozzle diameter, but the printing speed and dimensional resolution should be considered.

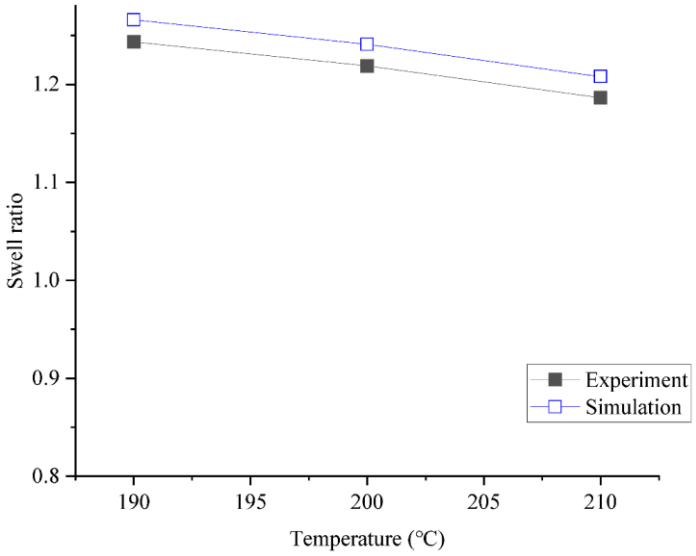

Fig.12 Effect of temperature on the swell ratio

5 Conclusion

The extrudate swell ratio of PLA in EAM process flowing through a nozzle was experimentally characterized. The processing parameters of temperature and extrusion rate, and the nozzle diameter were studied. The relations among the screw rotation speed, extrusion temperature and volume flow rate were determined, and the real values were taken as the input of numerical simulation.

The numerical simulation of extrudate swell of PLA was realized using the TPF module and LS method in COMSOL Multiphysics. The results of experiment and simulation agreed well showing a maximal error of 4%. Both results showed that the extrusion swell decreases with the increase of the extrusion temperature and the nozzle dimeter, and with the decrease of extrusion rate.

Statements and Declarations

Funding and acknowledgements

The authors gratefully acknowledged the financial support received from the China Scholarship Council (CSC). Experimental tests were carried out thanks to SupMicroTech-ENSMM workshop and local plateforms (AMETISTE for metrology and tribology, MIFHYSTO for cutting forces). This work was carried out within the Manufacturing 21 network, which gathers about 20 French research laboratories. The covered topics are the study and modelling of the manufacturing processes, especially the numerical simulation and investigation of extrudate swell of polylactic acid (PLA) via extrusion-based Additive Manufacturing process.

Competing Interest

The authors have no competing interests to declare that are relevant to the content of this article. This work was realized on a 3D printing equipment at the department of applied mechanics of Besançon, the presented results are free of commercial rights.

Author contributions

H. Wang: Design; Methodology; Data analysis; Visualization; Writing- Original draft.

F. Rabhi: Data analysis; Writing-Editing

A. Cherouat: Supervision; Review - Editing

A. Gilbin: Methodology

T. Barriere: Supervision; Review-Editing

References

[1] K. Rane and M. Strano, "A comprehensive review of extrusion-based additive manufacturing processes for rapid production of metallic and ceramic parts," *Adv. Manuf.*, vol. 7, no. 2, pp. 155–173, Jun. 2019, doi: 10.1007/s40436-019-00253-6.

[2] M. Van den Eynde and P. Van Puyvelde, "3D Printing of Poly(lactic acid)," 2017, pp. 139–158.

[3] S. Wickramasinghe, T. Do, and P. Tran, "FDM-Based 3D printing of polymer and associated composite: A review on mechanical properties, defects and treatments," *Polymers (Basel).*, vol. 12, no. 7, pp. 1–42, 2020, doi: 10.3390/polym12071529.

[4] N. Charpentier, T. Barrière, F. Bernard, N. Boudeau, A. Gilbin, and P. Vikner, "PIM-like EAM of steel-tool alloy via bio-based polymer," *Procedia CIRP*, vol. 108, pp. 477–482, 2022, doi: 10.1016/j.procir.2022.04.077.

[5] W. Hassan, M. A. Farid, A. Tosi, K. Rane, and M. Strano, "The effect of printing parameters on sintered properties of extrusion-based additively manufactured stainless steel 316L parts," *Int. J. Adv. Manuf. Technol.*, vol. 114, no. 9–10, pp. 3057–3067, Jun. 2021, doi: 10.1007/s00170-021-07047-w.

[6] J. Gonzalez-Gutierrez, S. Cano, S. Schuschnigg, C. Kukla, J. Sapkota, and C. Holzer, "Additive manufacturing of metallic and ceramic components by the material extrusion of highly-filled polymers: A review and future perspectives," *Materials (Basel).*, vol. 11, no. 5, 2018, doi: 10.3390/ma11050840.

[7] W. Sinthavathavorn, M. Nithitanakul, B. P. Grady, and R. Magaraphan, "Melt rheology and die swell of PA6/LDPE blends by using lithium ionomer as a compatibilizer," *Polym. Bull.*, vol. 63, no. 1, pp. 23–35, Jul. 2009, doi: 10.1007/s00289-009-0063-x.

[8] J. Z. Liang, J. Yang, and C. Y. Tang, "Die-swell behavior of PP/Al(OH)3/Mg(OH)2 flame retardant composite melts," *Polym. Test.*, vol. 29, no. 5, pp. 624–628, 2010, doi: 10.1016/j.polymertesting.2010.03.014.

[9] J. S. Anand and I. S. Bhardwaj, "Die swell behaviour of polypropylene - An experimental investigation," *Rheol. Acta*, vol. 19, no. 5, pp. 614–622, 1980, doi: 10.1007/BF01517515.

[10] E. Behzadfar, M. Ansari, V. K. Konaganti, and S. G. Hatzikiriakos, "Extrudate swell of HDPE melts: I. Experimental," *J. Nonnewton. Fluid Mech.*, vol. 225, pp. 86–93, Nov. 2015, doi: 10.1016/j.jnnfm.2015.07.008.

[11] L. A. Utracki, Z. Bakerdjian, and M. R. Kamal, "A method for the measurement of the true die swell of polymer melts," *J. Appl. Polym. Sci.*, vol. 19, no. 2, pp.

481–501, Feb. 1975, doi: 10.1002/app.1975.070190213.

[12] A. Dutta and M. E. Ryan, “A study of parison development in extrusion blow molding,” *J. Nonnewton. Fluid Mech.*, vol. 10, no. 3–4, pp. 235–256, Jan. 1982, doi: 10.1016/0377-0257(82)80003-7.

[13] D. Kalyon, V. Tan, and M. R. Kamal, “The dynamics of parison development in blow molding,” *Polym. Eng. Sci.*, vol. 20, no. 12, pp. 773–777, Aug. 1980, doi: 10.1002/pen.760201202.

[14] Y. Béreaux, J.-Y. Charmeau, and J. Balcaen, “Optical measurement and modelling of parison sag and swell in blow moulding,” 2011, pp. 683–688, doi: 10.1063/1.3589594.

[15] D. Tang, F. H. Marchesini, D. R. D’hooge, and L. Cardon, “Isothermal flow of neat polypropylene through a slit die and its die swell: Bridging experiments and 3D numerical simulations,” *J. Nonnewton. Fluid Mech.*, vol. 266, no. December 2018, pp. 33–45, 2019, doi: 10.1016/j.jnnfm.2019.02.004.

[16] R. I. Tanner, “A Theory of Die-Swell,” vol. 8, pp. 2067–2078, 1970.

[17] D. Tang, F. H. Marchesini, L. Cardon, and D. R. D’Hooge, “Three-dimensional flow simulations for polymer extrudate swell out of slit dies from low to high aspect ratios,” *Phys. Fluids*, vol. 31, no. 9, 2019, doi: 10.1063/1.5116850.

[18] V. K. Konaganti, M. Ansari, E. Mitsoulis, and S. G. Hatzikiriakos, “Extrudate swell of a high-density polyethylene melt: II. Modeling using integral and differential constitutive equations,” *J. Nonnewton. Fluid Mech.*, vol. 225, pp. 94–105, 2015, doi: 10.1016/j.jnnfm.2015.07.005.

[19] E. H. Tümer and H. Y. Erbil, “Extrusion-Based 3D Printing Applications of PLA Composites: A Review,” *Coatings*, vol. 11, no. 4, p. 390, Mar. 2021, doi: 10.3390/coatings11040390.

[20] A. Dervieux and F. Thomasset, “A finite element method for the simulation of a Rayleigh-Taylor instability,” 1980, pp. 145–158.

[21] S. Fedkiw, “Level set methods and dynamic implicit surfaces,” *Surfaces*, vol. 44, no. 77, 2002.

[22] J. A. Sethian, *Level Set Methods and Fast Marching Methods: Evolving Interfaces in Computational Geometry, Fluid Mechanics, Computer Vision, and Materials Science*. Cambridge University Press, 1999.

[23] D. O. Kazmer, A. R. Colon, A. M. Peterson, and S. K. Kim, “Concurrent characterization of compressibility and viscosity in extrusion-based additive manufacturing of acrylonitrile butadiene styrene with fault diagnoses,” *Addit. Manuf.*, vol. 46, p. 102106, 2021, doi: 10.1016/j.addma.2021.102106.

[24] M. Hyvärinen, R. Jabeen, and T. Kärki, “The modelling of extrusion processes for polymers-A review,” *Polymers (Basel).*, vol. 12, no. 6, 2020, doi: 10.3390/polym12061306.

[25] D. A. Anderegg *et al.*, “In-situ monitoring of polymer flow temperature and pressure in extrusion based additive manufacturing,” *Addit. Manuf.*, vol. 26, no. January, pp. 76–83, 2019, doi: 10.1016/j.addma.2019.01.002.

[26] M. P. Serdeczny, R. Comminal, D. B. Pedersen, and J. Spangenberg, “Experimental and analytical study of the polymer melt flow through the hot-end in material extrusion additive manufacturing,” *Addit. Manuf.*, vol. 32, no. October 2019, p. 100997, Mar. 2020, doi: 10.1016/j.addma.2019.100997.